1   The ST22 chronology for the Skytrain Ice Rise ice core - part 2: an age model to the last interglacial

2   and disturbed deep stratigraphy.

3   **Authors**: Robert Mulvaney[1], Eric W. Wolff[2], Mackenzie M. Grieman[2,3], Helene H. Hoffmann[2], Jack D.

4   Humby[1], Christoph Nehrbass-Ahles[2], Rachael H. Rhodes[2], Isobel F. Rowell[2], Frédéric Parrenin[4], Loïc

5   Schmidely[5], Hubertus Fischer[5], Thomas F. Stocker[5], Marcus Christl[6], Raimund Muscheler[7], Amaelle

6   Landais[8], Frédéric Prié[8]

7

8   1. British Antarctic Survey, Cambridge, UK

9   2. Department of Earth Sciences, University of Cambridge, UK

10   3. Reed College, Portland, Oregon, USA

11   4. Université Grenoble Alpes, CNRS, IRD, Grenoble INP, IGE, 38000 Grenoble, France

12   5. Climate and Environmental Physics, Physics Institute, and Oeschger Centre for Climate Change

13   Research, University of Bern, Switzerland

14   6. Laboratory for Ion Beam Physics, ETH Zurich, 8093 Zurich, Switzerland

15   7. Department of Geology, Quaternary Sciences, Lund University, Sölvegatan 12, SE-22362 Lund,

16   Sweden

17   8. Laboratoire des Sciences du Climat et de l'Environnement, LSCE/IPSL, CEA-CNRS-UVSQ, Université

18   Paris-Saclay, Gif-sur-Yvette, France

19   Correspondence to: Eric Wolff (ew428@cam.ac.uk)

20

21   Abstract

22   We present an age model for the 651 m deep ice core from Skytrain Ice Rise, situated inland of the

23   Ronne Ice Shelf, Antarctica. The top 2000 years have previously been dated using age markers

24   interpolated through annual layer counting. Below this, we align the Skytrain core to the AICC2012

25   age model using tie points in the ice and air phase, and apply the Paleochrono program to obtain the

26   best fit to the tie points and glaciological constraints. In the gas phase, ties are made using methane

27   and, in critical sections, $\delta^{18}O_{air}$; in the ice phase ties are through ^{10}Be across the Laschamps Event,

28   and through ice chemistry related to long-range dust transport and deposition. This strategy

29   provides a good outcome to about 108 ka (~605 m). Beyond that there are signs of flow disturbance,

30   with a section of ice probably repeated. Nonetheless values of CH_4 and $\delta^{18}O_{air}$ confirm that part of

31   the last interglacial (LIG), from about 117-126 ka (617-627 m), is present and in chronological order.

32   Below this there are clear signs of stratigraphic disturbance, with rapid oscillation of values in both

33   the ice and gas phase at the base of the LIG section, below 628 m. Based on methane values, the

34   warmest part of the LIG and the coldest part of the penultimate glacial are missing from our record.

35   Ice below 631 m appears to be of age >150 ka.

36

37   1.   Introduction

38

39   There is currently intense interest in the role of the Antarctic Ice Sheet, and the West Antarctic Ice

40   Sheet (WAIS) in particular, in future sea level rise (DeConto et al., 2021; Fox-Kemper et al., 2021).

41   While modern studies of the behaviour of the WAIS are essential, studies aimed at assessing the past

42   stability of the WAIS and its response to past climate change are required to constrain the operation

43   of proposed feedbacks (such as the Marine Ice Cliff Instability mechanism) (Gilford et al., 2020). The

44   last interglacial (LIG, Marine Isotope Stage (MIS) 5e, ~130-110 ka before present (bp) where present

45   is defined as 1950) has been considered of particular interest because estimates of sea level during

46   that period compared to the present (Dutton et al., 2015; Dyer et al., 2021) appear to require some

47   contribution from retreat of the Antarctic Ice Sheet. In order to assess the sensitivity of the WAIS

48   and its surrounds to climate change, it is also of interest to understand how the climate and the ice

49   in the WAIS region responded to the coolings and warmings of the last glacial period and the

50   warming into the Holocene.

51   While there are a number of Antarctic ice core records extending through at least one climate cycle

52   and into the LIG from East Antarctica (e.g. Crotti et al., 2021; EPICA Community Members, 2004;

53   Grootes et al., 2001; Kawamura et al., 2007), long records from West Antarctica are scarce. The

54   WAIS Divide ice core (Fig. 1) provides an excellent and well-resolved record of the last 68 kyr (Buizert

55   et al., 2015) but does not extend further back in time. The only other long core in the interior of the

56   WAIS is the 2191 m long Byrd core, for which the oldest ages presented are 90 ka (Ahn and Brook,

57   2008). On the periphery of the WAIS, the Siple Dome core reached the bed at 1004 m, but again data

58   have only been presented as far back as 100 ka (Brook et al., 2005; Saltzman et al., 2006;

59   Severinghaus et al., 2009). At Roosevelt Island, situated within the Ross Ice Shelf, the ice could not

60   yet be dated beyond 83 ka (Lee et al., 2020). Old ice might be available at the bottom of the Berkner

61   Island (Mulvaney et al., 2007) and Fletcher Promontory (Mulvaney et al., 2014) cores, but there is no

62   published age scale for these cores so far.

63

Figure 1. Map showing ice core sites in West Antarctica that are mentioned in text. Map generated using QGIS with the Quantarctica mapping environment (Matsuoka et al., 2021).

The only record that seems to unequivocally reach the LIG in West Antarctica to date is that from a horizontal ice trench in the blue ice area at Mount Moulton (Korotkikh et al., 2011). This appears to reach 135 ka, although the nature of the record makes it hard to assess its continuity. It is therefore a priority to find sites in the WAIS vicinity where a record extending to the LIG can be retrieved and fully analysed. One potential candidate site, near the boundary between the East and West Antarctic Ice Sheets, would be Hercules Dome (Jacobel et al., 2005), and drilling is expected there in the next few years. In this paper we present an age scale for an ice core drilled at Skytrain Ice Rise, at the boundary of the WAIS and the Ronne Ice Shelf.

74   The core at Skytrain Ice Rise was drilled to the bed at 651 m depth in 2018-19 (Mulvaney et al.,

75   2021). Skytrain Ice Rise (Fig. 2) is an independent ice rise (i.e., with its own flow regime) with a

76   circular shape and a diameter of ~80 km. It sits at an altitude of 784 m, has a 10 m temperature

77   (representing mean annual temperature today) of -25.9°C, and a basal temperature of -14.9°C. It

78   represents an attractive target because its isotopic and chemical content should be sensitive to

79   changes in the extent and altitude of the WAIS, and also to the extent of the adjacent Ronne Ice

80   Shelf. It is situated on a bed that is above sea level, but surrounded almost entirely by ice shelf

81   (including Constellation and Hercules Inlets, see Fig. 2) that has a sea bed depth of at least 1000 m.

82   On the WAIS side, it is protected by the Ellsworth Mountains. This combination ensures that Skytrain

83   Ice Rise will almost certainly have remained as a separate ice dome, and would never have been

84   overridden by inland ice, whatever the size of the WAIS.
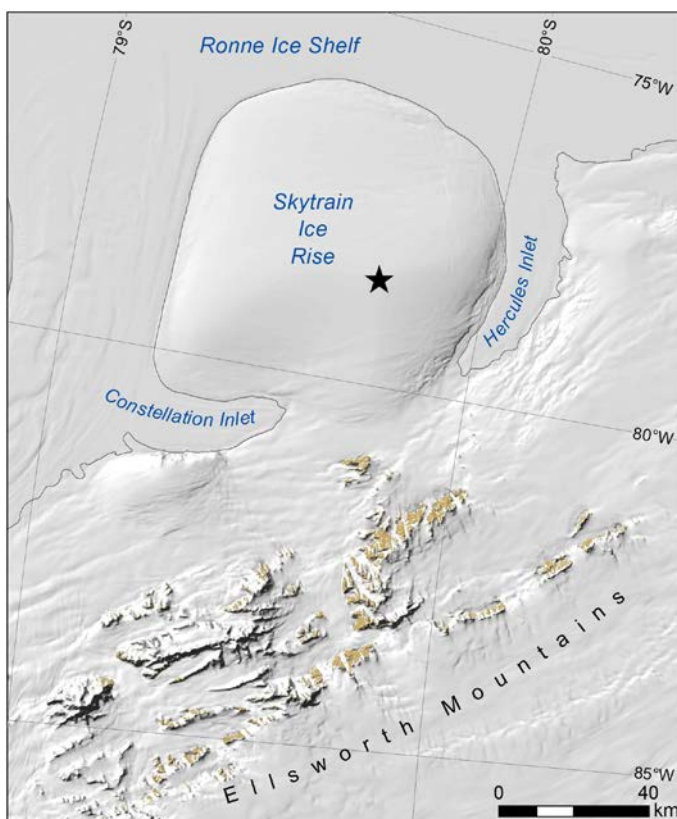
85

86   Figure 2. Skytrain Ice Rise. The drill site is marked with a star. Figure reproduced from (Mulvaney et

87   al., 2021), CC BY 4.0

88   Radar data collected previously showed good layering almost to the bed (Mulvaney et al., 2021),

89   with a pronounced Raymond Arch. The drill site was chosen based on the radar layers to give old ice

90   as far from the bed as possible.

91 In a companion paper to this one (Hoffmann et al., 2022) we have used a variety of age markers,

92 interpolated through counting of annual layers in chemistry, to derive an age scale for the last 2000

93 years (~200 m). In this paper we use a range of evidence to derive an age model for the rest of the

94 core. In particular, we demonstrate that the core contains an intact record of the last glacial period

95 and extends into the LIG. We also discuss the possible age of more disturbed ice found in the

96 deepest twenty metres of the core.

97

98 2. Overall dating strategy

99 The strategy, as with other recent dating papers (Epifanio et al., 2020), is to tie the Skytrain Ice Rise

100 core to a well-established age model. Since we expected our core to run well beyond the age of the

101 WAIS Divide core, we have chosen to give our final derived ages as those of the AICC2012 age model

102 (Bazin et al., 2013; Veres et al., 2013), which was developed for the EPICA ice cores but includes

103 synchronized age scales for some of the major East Antarctic Ice Sheet deep ice cores (Talos Dome,

104 Vostok) and which is synchronized to the Greenland NGRIP ice core in the upper 60 kyr. However,

105 we recognise that the WD2014 age model (Buizert et al., 2015; Sigl et al., 2016), developed for the

106 WAIS Divide ice core) is more accurate in absolute age over the last 68 kyr, and that methane data

107 are available at a much higher resolution in cores that have been tied to it. For that reason, in some

108 cases we initially matched our core to WD2014 and then used a simple translation table to tie it to

109 AICC2012. For convenience, our depth-age table in the supplement provides both WD2014 and

110 AICC2012 ages for the last 63 kyr. This is based on volcanic synchronisations (Buizert et al., 2018; Sigl

111 et al., 2022) for the age of the ice.

112 In order to construct the age alignment, and estimate uncertainty, we use the Paleochrono program

113 which is a development of the Icechrono program (Parrenin et al., 2015). We include a number of

114 stratigraphic alignments to AICC2012, based on the data in the companion paper for the uppermost

115 2000 years, and using CH_4, $\delta^{18}O_{air}$, ^{10}Be, and ice chemistry markers in deeper ice. Paleochrono was

116 started with a prior for the accumulation rate (based on a simple relationship with water isotope

117 ratios), air lock-in depth and a simple ice thinning function. Paleochrono minimises a cost function

118 that measures the misfit of the model with respect to the prior and the observations (tie points).

119 2.1. Flow disturbance

120 In the deeper part of the ice core, between 628-635 m, we observe some discontinuities, with rapid

121 and simultaneous changes in water isotopes and methane at the same depth. These will be

122 discussed in more detail later, but they represent likely depths of flow disturbance or folding, as has

123 been observed in other ice core records, including those of the LIG in Greenland (Chappellaz et al.,

124 1997; NEEM Community Members, 2013; Yau et al., 2016). We also deduce that some disturbance

125 may exist in a region between about 605 and 615 m depth. From 600 m downwards we therefore

126 carefully examine individual data points (using paired values of CH_4 and $\delta^{18}O_{atm}$ matched against

127 reference data) to reconstruct discrete ages for particular depths. This allows us to assess which

128 sections are in order with well-constrained ages, and which are disturbed in the deeper ice. We then

129 use Paleochrono to derive a continuous age model to 628 m, making manual adjustments to the

130 final age scale to avoid assigning spurious ages to data in the disturbed section.

131

132 3. Data available

133

134 In this section we describe the collection of the data used to make ties to other cores, both in the

135 gas phase (air bubbles) and in the ice phase.

136

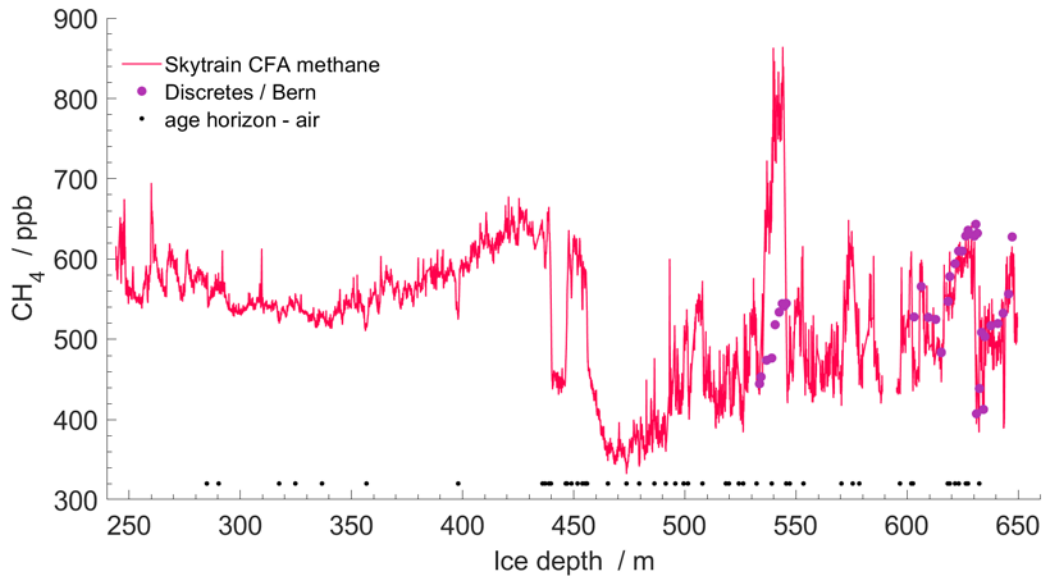137   3.1. Continuous methane

138 Methane measurements are a particularly powerful way of aligning the gas ages of different ice

139 cores because they exhibit large (from tens to 200 ppb) and abrupt changes of concentration across

140 millennial-scale Dansgaard-Oeschger events that recur throughout the last glacial period (e.g.

141 Epifanio et al., 2020). Using high-resolution continuous analysis it has also been shown that

142 centennial and faster variability down to below 10 ppb amplitude is well-reproduced between cores

143 (Lee et al., 2020; Mitchell et al., 2013; Rhodes et al., 2017). As methane is well-mixed in the Antarctic

144 troposphere, not just the pattern but the absolute values should match with reference datasets

145 within uncertainty. Our main dataset, from continuous flow analysis (CFA), is good at showing the

146 high-resolution variability, but has a large and unknown uncertainty in absolute values. We therefore

147 supplement it with some discrete analyses (section 3.2) that constrain the concentration tightly at

148 key sections of ice.

149 We measured methane (CH_4) continuously during the continuous flow analysis (CFA) campaign

150 (Grieman et al., 2021). Briefly, the core was melted at a mean rate of 3.2 cm min^{-1} and the air was

151 separated from residual water flow using a 3M Liqui-Cel MM-0.5x1 Series membrane contactor. The

152 dried air was then directed to a Picarro G2301 CRDS for CH_4 analysis. While the methane Picarro

153 calibration could not be checked against external certified standards, comparison of our data

154 produced by CFA with analysis of discrete samples analysed in Bern (section 4.2), as well as

comparison of our CFA data with reference data across the Holocene and glacial, suggests that the CFA methane reproduces the variability in methane at centennial scales. However, the absolute values are offset (mainly low) by an amount that varied by a few percentage points over the campaign but the offset was typically below 10%. This offset arises partly from dissolution of a small percentage of gas into the meltwater stream, as has been observed previously using CFA to measure methane (Rhodes et al., 2015). Continuous analyses started at 244 m depth and continued in all sections where the ice was of suitable quality to 649.4 m. A short section from 144.0-161.3 m was also analysed continuously for methane with an improved measurement setup which is discussed in the companion paper (Hoffmann et al., 2022).

Two significant issues affected the measurements. Firstly, a section of data between 534 and 545 m was affected by a leak of lab air at the membrane contactor. The absolute values in this section of ice are therefore substantially higher than palaeoatmosphere, but the pattern of variability can still partly be used for wiggle-matching after correction using discrete analyses (next section).

A second issue is that there were increasing numbers of breaks and cracks in the ice with depth, particularly below 450 m. Badly cracked sections were removed before the ice was placed on the melter and breaks across the core were smoothed with a cleaned file to ensure that the contact between ice sections was as close as possible. With these precautions, such occurrences do not affect the ice phase chemical measurements and most do not affect CH_4 either. Nonetheless some of the remaining cracks and transitions between different bags provide an opportunity for the ingress of lab air as the ice melts, leading to spikes in methane concentration. Major short peaks and troughs were identified manually, and removed from the dataset. Above 500 m ~25 spikes that were at least a factor 2 higher or lower than the mean of the dataset were removed. Below 500 m, the data became much noisier and ~100 deviations from the dataset were manually removed. Even after removal of the obvious spike artefacts the data remain more noisy than the data that are unaffected by such artefacts, suggesting that positive artefacts arising from inclusion of modern air remain in the dataset. This makes it trickier to clearly align data with a reference dataset in the deeper ice. The dataset below 244 m is shown in Fig 3.

Figure 3. Continuous (CFA) methane (red line), and data from discrete measurements (purple dots), after removal of occasional methane spikes as discussed in the text. The discrete data confirm that the continuous data between 534 and 545 m are offset, and confirm that the uncalibrated values for the remaining continuous data are reasonable. Tie points used to construct the age scale are shown as black dots.

3.2. Discrete methane

To validate and control that the absolute levels of our continuous CH_4 record are consistent within uncertainty with the absolute values in reference data, we obtained some well-calibrated discrete measurements (Fig. 3), particularly in the deep ice and in the section impacted by the air leak (section 3.1). Ten discrete samples were therefore measured at the University of Bern between 533-546 m, and a further 25 samples between 600 and 650 m depth. Details of the method have been published elsewhere (Schmidely et al., 2021). Concentrations ranged between 413 and 644 ppb, with an estimated precision (1 sigma) of 7 ppb (Table S1). Note that the discrete data presented here have been corrected by -18 ppb (Schmidely et al., 2021) to align them with previously published CH_4 records. These offsets are potentially due to different remnant solubility of CH_4 in meltwater using different melt extraction methods in different labs. Taking the uncertainty of the correction into account, the total uncertainty is estimated at 12 ppb (Schmidely et al., 2021), while that of the reference data is estimated at 10 ppb (Loulergue et al., 2008). Combining these uncertainties suggests that when comparing absolute values of methane (discrete data) with reference datasets we should allow an uncertainty of 16 ppb (much higher offsets are possible for the data derived by CFA, and there we mainly look for similar patterns to those in the reference data). The discrete data measured in Bern are displayed along with the continuous data in Fig. 3 and in Fig. S1. A number of

8

205   discrete measurements were also made between 84 and 144 m at Oregon State University which are

206   described in the companion paper (Hoffmann et al., 2022).

207   3.3. $\delta^{18}O$ of O_2 ($\delta^{18}O_{atm}$)

208   The isotopic ratio of oxygen in air provides a good additional constraint because it is well-mixed

209   globally, and varies in line with precession, providing opportunities for aligning measurements with

210   calculated orbital targets as well as with measurements from other ice cores (Extier et al., 2018).

211   CH_4 and $\delta^{18}O_{atm}$ have previously been used powerfully in tandem to untangle disturbed ice

212   chronologies in the LIG (Chappellaz et al., 1997; Yau et al., 2016).

213   In this work, 27 samples were analysed for $\delta^{18}O_{atm}$ at the Laboratoire des Sciences du Climat et de

214   l'Environnement (LSCE). Two samples were in the depth range 160-170 m, and 5 were between 435

215   and 471 m. The remaining samples were in the depth range 602-635 m. Data were corrected for firn

216   fractionation and gas loss (Extier et al., 2018) and are shown in Table S1; data below 600 m are

217   shown on a depth scale in Fig. S1. Uncertainty on each value is estimated at +/- 0.03 ‰. Combining

218   this with the similar uncertainty in data points in the reference dataset suggests that we should

219   allow an uncertainty of 0.04‰ when comparing our data with the reference.

220   3.4. ^{10}Be across the Laschamps Event

221   The flux/concentration of ^{10}Be in ice shows a pattern related to variations in the magnetic field of

222   the Sun and, on longer timescales, Earth. The pattern of these variations can be matched between

223   ice cores, and with ^{14}C variations in other archives such as tree rings, in order to synchronise records

224   (e.g. Adolphi and Muscheler, 2016). A particularly clear and prominent pattern is seen across the

225   Laschamps Event, a weakening of Earth's magnetic field that occurred around 41 ka bp (e.g. Raisbeck

226   et al., 2017). Because this section of ice is in the last glacial period, its synchronisation in the ice

227   phase should allow for a particularly useful and unambiguous estimate of the offset between ice age

228   and gas age (Δage) in the glacial period.

229   Seventy samples from between 509 and 520 m depth were spiked with a known amount of ^9Be,

230   processed in Lund and analysed for ^{10}Be by Accelerator Mass Spectrometry at ETH Zurich. Measured

231     $^{10}Be/^9Be$ ratios were normalized to the ETH Zurich in-house standards S2007N and S2010N with

232   nominal $^{10}Be/^9Be$ ratios of 28.1 x 10^{-12} and 3.3 x 10^{-12} (Christl et al., 2013). Data and associated

233   uncertainties are presented in Table S2.

234   3.5. Aluminium (Al) and non sea salt magnesium (nssMg)

235   When synchronising ice cores from different sites, it is important to use only parameters for which

236   there is a sound reason to assume that both cores share synchronous variability. This is the case, for

237   example, with volcanic eruption spikes, with [10]Be and with well-mixed atmospheric gases, such as

238   methane. It is not safe to make such an assumption for water isotopes, which are site-dependent

239   because climatic changes may vary asynchronously in different parts of Antarctica. While methane

240   synchronisation (see above) and a relatively small Δage compared to inland sites (due to the higher

241   accumulation rate) allows us to make a reasonable estimate of the ice age along our core, it would

242   be advantageous to have further ties in the ice phase. It has been argued previously that variations

243   in the components of terrestrial dust (such as Ca) can be assumed to be synchronous across

244   Antarctica (Baggenstos et al., 2018; Mulvaney et al., 2000). This is because their concentrations are

245   strongly controlled by events at a common source in South America and in a common part of the

246   transport pathway towards Antarctica, with only a minor part of the variability likely to be

247   dependent on the final stages of transport to each ice core site.

248   The main component used for such synchronisation to date has been non-sea-salt (nss) Ca,

249   calculated using marine and terrestrial ratios of Ca and Na (e.g. Röthlisberger et al., 2002)). However,

250   after an initial attempt we observed that while nssCa at Skytrain Ice Rise shows a good coherence

251   with that of other sites (EDC, EDML) until a depth of about 500 m (30 ka bp), it diverges below that.

252   Other terrestrial markers such as Al and nssMg (calculated as Mg-0.12*Na and both measured by

253   ICP-MS during the CFA campaign (Grieman et al., 2021)) do not mirror the Skytrain nssCa signal, and

254   do appear to follow nssCa at other East Antarctic sites (see section 5.3). It appears that an additional

255   source of Ca-rich material, not seen in other Antarctic cores and presumably due to local sources, is

256   present at this site in the earlier part of the last glacial. The reasons for this will be explored

257   elsewhere. However, the solution for us is to use the terrestrial markers that appear free from this

258   extra source, but that are coherent with nssCa records at other sites. The limits of detection of Al

259   and Mg are 3.3 ppb and 1.3 ppb, respectively. We concentrate on alignments from nssMg because a

260   majority of Al values in the Holocene and marine isotope stage 5 fall below the detection limit; in the

261   glacial the Al values support our conclusions with nssMg.

262   4.   Reference datasets

263   Since the basis for our age model is tying variations in our data to variations in well-dated ice cores,

264   in this section we describe the reference datasets used.

265   4.1. Gas phase: Methane and $\delta^{18}O$ of O_2 ($\delta^{18}O_{atm}$)

266   In order to use the more detailed variability that can be traced during the Holocene, we compared

267   our methane data to the high resolution Roosevelt Island methane record between 2-7 ka bp.

268   Between 7-68 ka we used the WAIS Divide record (Buizert et al., 2015; Rhodes et al., 2017). Between

269   68 and 156 ka, we used the southern hemisphere methane spline generated from the EDC ice core

270   (Köhler et al., 2017). To investigate possible matches with older ice we used the EDC data itself

271   (Loulergue et al., 2008). As previously explained, the Roosevelt and WAIS Divide data are on the

272   WD2014 age scale, but we eventually used a conversion table (based on Buizert et al., 2018) to place

273   all matches onto a common AICC2012 age scale.

274   A composite EDC-Vostok record of $\delta^{18}O_{atm}$ (Extier et al., 2018) was used for comparison to Skytrain

275   ice core $\delta^{18}O_{atm}$.

276   4.2. Ice phase: ^{10}Be across the Laschamps Event and terrestrial marker elements

277   The clear pattern of the ^{10}Be record across the Laschamps Event has been shown to be closely

278   replicated at several sites in Greenland and Antarctica (Raisbeck et al., 2017). For the

279   synchronisation, we used the normalised stack that was recently created based on 3 Greenland and

280   3 Antarctic records (Adolphi et al., 2018).

281   As the reference dataset for terrestrial deposition we used the nssCa record from EDML (Fischer et

282   al., 2007), because of its greater proximity to Skytrain in the Atlantic sector of Antarctica, with

283   further validation using the record from EDC (Wolff et al., 2010).

284   5. Tie points to 100 ka

285   5.1. Methane

286   First, we note that the discrete methane data (Fig. 3) confirm that the methane concentrations in

287   the section from 534-545 m are much too high. In this section of ice we therefore use the values

288   from the discrete data to match with reference data.

289   In Table S3, we list the methane tie points that we used in this section. The very clear match

290   between our record and the reference data is ideally seen in the past 15 kyr (460 m) where there are

291   few spikes in the methane record due to air ingress into cracks (Fig. 4). However, the pattern of

292   Dansgaard-Oeschger events remains clear right down to 100 ka, and is shown in Fig. 5, along with

293   the tie points used. We note that the comparisons in Fig. 4 suggest that the Skytrain data might be

294   up to 10% too low in concentration (but with a variable offset along the core) compared to the

295   reference data; this results from the dissolution of gas in the meltstream (as discussed in section 3.1)

296   and the difficulty of accurately calibrating data from the continuous melter due to the absence of an

297   external certified standard. In Fig. 5 we show the full methane record on the eventual age scale,

298   compared to reference data. It is clear that some spikes due to air ingress across cracks remain in the

299   dataset beyond about 60 ka, but the pattern for matching is still apparent to at least 100 ka. The

300   match between Skytrain and reference methane between 80 and 100 ka is less secure than it is in

301   shallower ice, because ice with high concentration outliers and/or missing data is common as a

302   result of extensive cracking. This makes it hard to match absolute values of methane, and forces us

303   to rely on the pattern with depth. Nonetheless, the methane ties we have made result in a good

304   match in this part of the core between nssMg and reference nssCa (Fig. 7 and section 5.3),

305   supporting our choices. The section beyond 100 ka will be discussed in section 6.

306
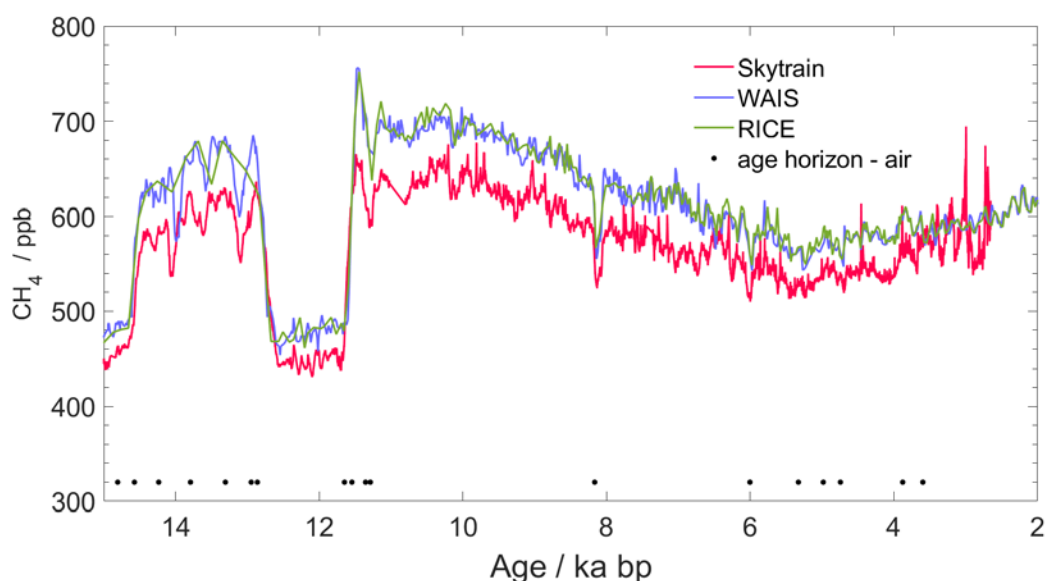
308   Figure 4. Methane matching over the last 15 kyr. Methane from Skytrain Ice Rise (red) on its age

309   scale after synchronisation, along with methane from Roosevelt Island (green) (Lee et al., 2020), and

310   WAIS Divide (blue) (Buizert et al., 2015; Mitchell et al., 2013). Ages shown here are WD2014. The

311   concentration offset between the Skytrain and other data is probably caused by partial dissolution in

312   the meltstream for Skytrain as discussed in the text. Tie points used to construct the age scale are

313   shown as black dots.

314
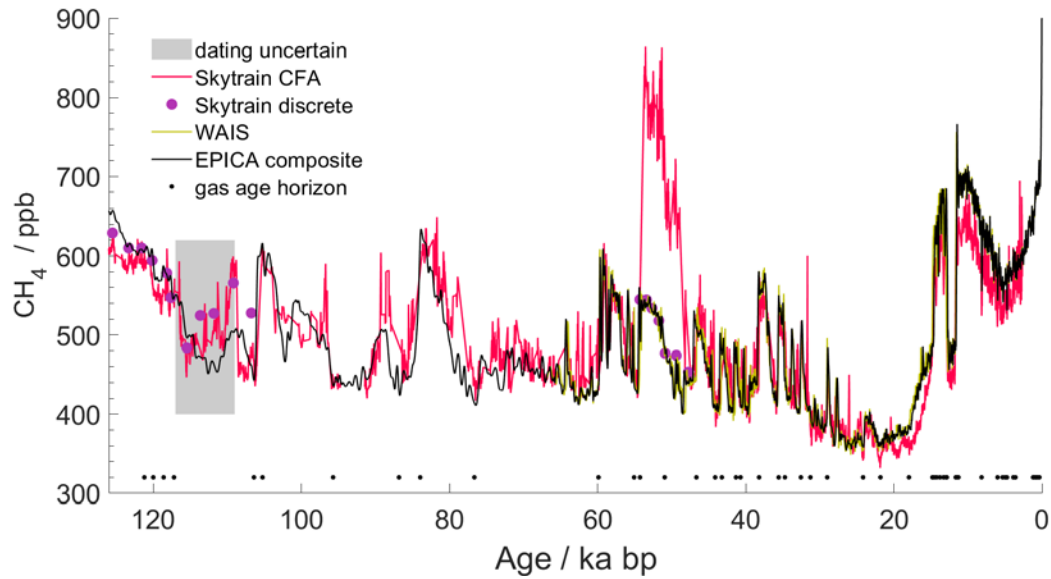
Figure 5. Methane from Skytrain Ice Rise on the ST22 age scale, along with reference data. Skytrain is shown in red line (continuous) and purple dots (discrete data). In black is a spline of Antarctic data (Köhler et al., 2017). WAIS Divide is shown in yellow (Buizert et al., 2015; Mitchell et al., 2013). Ages shown here are AICC2012. Gas age tie points are shown along the bottom of the figure. The grey shaded area represents the ice (605-617m) with unreliable ages due to flow disturbance (see section 8).

5.2. ^{10}Be across the Laschamp Event

In Fig. 6 we show the Skytrain ^{10}Be concentration from 509-520 m, aligned with the reference dataset. The common shape across the wider event as well as the presence of individual peaks and troughs is clear. We chose 5 tie points in the range 39.9-42.0 ka bp (Table S4).

13

325
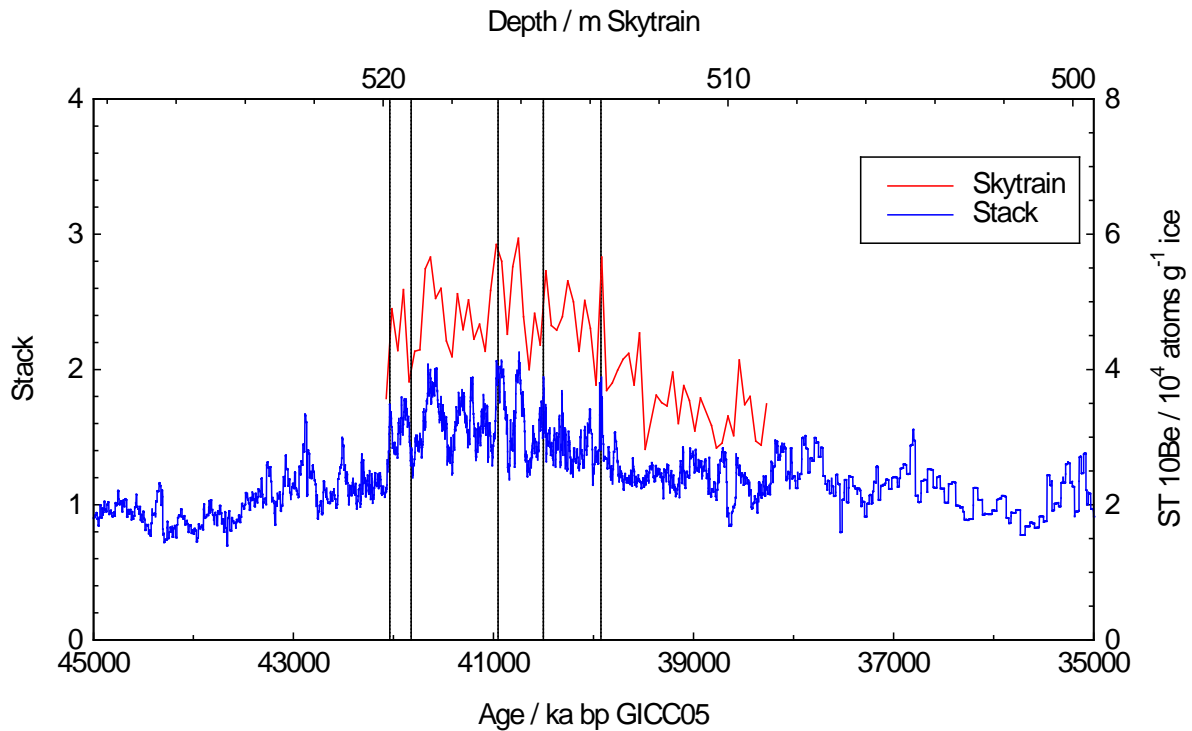
Figure 6. [10]Be concentration in the Skytrain (ST) ice core (red) compared to the normalised stack of ice core radionuclide data (Adolphi et al., 2018). Two samples with obvious low outlier concentrations in the ST record have not been plotted. Vertical lines show the tie points used in this study.

5.3. nssMg compared to Ca at EDML

Skytrain nssMg was compared to nssCa from EDML (Fischer et al., 2007) (Fig. 7). The two records show strong similarities, as does Skytrain Al (not shown) where it exceeds the detection limit; comparison with EDC nssCa (Wolff et al., 2010) shows a comparably good match. We chose a few obvious tie points (Table S4) concentrating on regions with clear variability and trying to fill the gaps where fewer ice tie points existed. We discuss the ice below 100 ka in section 6.
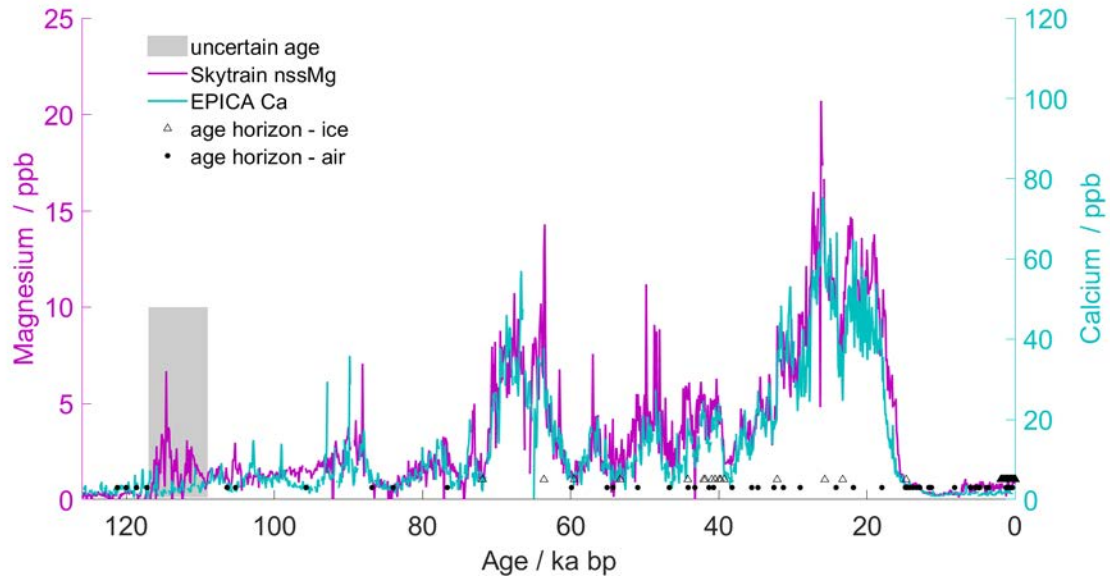
Figure 7. nssMg at Skytrain shown on its age scale after synchronisation (purple). nssCa from EDML (cyan) (Fischer et al., 2007). Tie points used in this paper are shown (circles are gas age, triangles are ice age ties). The grey shaded area represents the ice (605-617m) with unreliable ages due to flow disturbance (see section 8).

6. Dating the ice older than 100 ka

Below about 600 m (100 ka), methane continues to show a pattern similar to that of the reference record, with a peak between 600-603 m (Fig. 3) that seems to correspond to the methane peak associated with Greenland interstadial (GI) 24 at 102-107 ka (Baumgartner et al., 2014; Capron et al., 2010). However below this, between 605-608 m, there is a further methane peak that appears anomalous: its concentrations are too high to match the reference data at GI 25. Whereas methane peaks typically have a sharp jump in concentration at their old (deeper) side, this peak has a sharp drop at its shallower side. From 616 to 622 m, methane rises in a stepped fashion similar to the increase seen in the reference record on the young side of the LIG between 114 and 123 ka, before plateauing (~625-629 m) at concentrations typical of the last interglacial (as confirmed by the discrete measurements made in Bern, with several concentrations between 630 and 644 ppb). However there are no values (in either the continuous or discrete data) that reach those (going above 700 ppb) that are seen in the reference data in the early last interglacial peak between 127 and 129 ka. Additionally, methane experiences a rapid alternation of values (two values > 600 ppb surrounding a value of 400 ppb within a metre) at 631 m (the base of the values that appear to be interglacial). This coincides (in depth) with a rapid alternation in water isotope ratios (not shown here). Finally there are also very few values below 400 ppb that would correspond to the low values seen in the reference data during the penultimate glacial maximum between about 140-145 ka.

360   These observations suggest that the ice is in good chronological order to 107 ka and probably from

361   about 117-126 ka, but that there might be a flow disturbance between 107 and 117 ka, and a

362   definite disturbance and discontinuity at the base of the last interglacial ice with some thousands of

363   years potentially missing from our record. Later we speculate on the reasons for this. For now it

364   causes us to be concerned about the integrity of the record above this depth (ie the LIG to 126 ka). It

365   suggests that the use of simple pattern matching of methane and nssMg in the LIG ice might risk a

366   false assignment, and so instead we seek a more definite quantitative match.
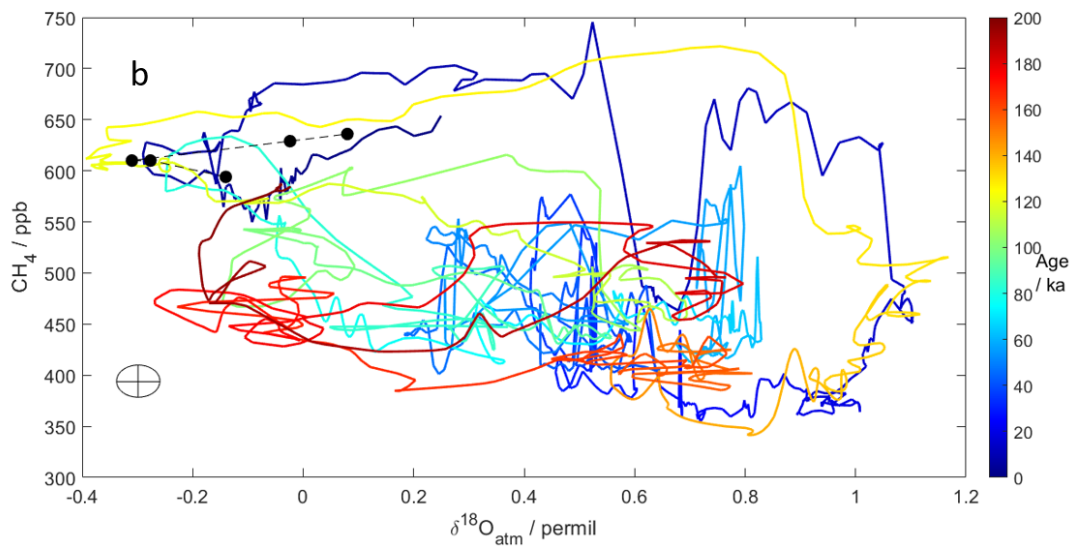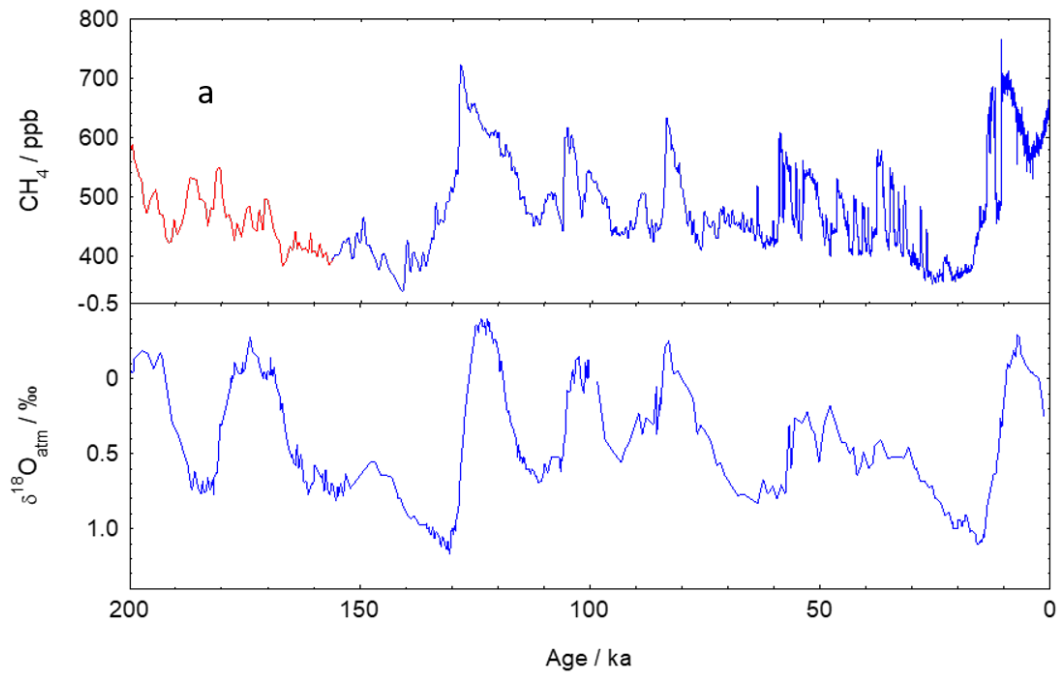
367   6.1. CH_4 and $\delta^{18}O_{atm}$

368   Flow disturbances affecting LIG ice have been seen previously, though until now this has been

369   observed mainly in Greenland. To confirm the age of ice with difficult stratigraphy, and even to re-

370   order disordered layers, previous authors have used a combination of methane and $\delta^{18}O_{atm}$

371   (Chappellaz et al., 1997; NEEM Community Members, 2013; Yau et al., 2016). Provided data are

372   sufficiently precise, the two-dimensional field of these parameters can define an age for a given

373   layer that is close to unique within the plausible range. In Fig. 8a we show the reference data for CH_4

374   and $\delta^{18}O_{atm}$.

375

376   By plotting the two-dimensional distribution of values (Fig. 8b) one can see how the data clearly

377   differentiate samples of different ages – this is particularly true in the section from about 120-140 ka

378   (section that goes clockwise in increasing age coloured yellow). While the $\delta^{18}O_{atm}$ data were used

379   mainly in combination with CH_4 to assess the ages of ice around the LIG, $\delta^{18}O_{atm}$ was also measured

380   in two Skytrain ice core samples from the Holocene and two from the last glacial maximum: these

381   were not used to construct the age scale but the values were entirely consistent with the modelled

382   ages. Three samples were also measured between 435 and 456 m. These three values of $\delta^{18}O_{atm}$,

383   along with the less precise CH_4 data obtained from the continuous measurements, were used to

384   assign ages (Table S1) more precisely between 11 and 15 ka in a section in which $\delta^{18}O_{atm}$ is increasing

385   rapidly with age (Fig. 8).

386

Figure 8. Reference data for CH$_4$, and δ^{18}O$_{atm}$ (Extier et al., 2018) over the last 200 ka. Data are all on the AICC2012 age model. (a) The two datasets as time series. CH$_4$ to 156 ka in blue (Köhler et al., 2017), beyond 156 ka in red (Loulergue et al., 2008) (b) Cross plot of CH$_4$ and δ^{18}O$_{atm}$ reference data for the period 0-200 ka. The colourbar indicates the age of the sample. The combined uncertainty is shown by the grey ellipse/cross. An alternative visualisation of panel b is provided in Fig. S5. The black dots are data from Skytrain Ice Rise from 621.5 to 627.3 m (following the dashed line clockwise).

Twenty Skytrain ice core samples were analysed for δ^{18}O$_{atm}$ between 600 and 635 m depth, covering the period that the discussion above would lead us to expect is older than 100 ka. In all but two

398   cases discrete methane measurements were made (in Bern) on an adjacent sample (a few cm away

399   from the $\delta^{18}O_{atm}$ sample).

400   We now examine the data at depths for which we have both $\delta^{18}O_{atm}$ and methane measurements.

401   We start with the data from 603-618 m (Fig. 9a). The data point at 603.1 m can be assigned an age of

402   ~106 ka, as we had already deduced above from the shape and amplitude of the methane peak

403   alone. While the point at 606.4 m matches best with ~118 ka, the 3 data points deeper than that

404   (609-618 m) are only compatible with younger ages, between 106 and 117 ka. We cannot untangle

405   this section but there is apparently some degree of disturbance at least between 605 and 615 m.

406   We have no reason to doubt that the ice is in good order until 605 m, but we acknowledge that the

407   section we date as 95-107 ka (Figs. 5, 7) relies on the pattern of methane and on a single CH$_4$/

408    $\delta^{18}O_{atm}$ datapoint. This point, dated at 106 ka, firmly defines the lower end of this section, with

409   values that do not occur again as a pair until 57 ka.

410   Turning now to Fig. 9b, the data from 615.3 to 627.3 m plot in chronological sequence with respect

411   to the reference data between about 110-126 ka. Most of these points are not consistent with

412    $\delta^{18}O_{atm}$ and methane values at any other ages in the range, 60-180 ka. Crucially the two datapoints

413   at 623.2 and 624.7 m with very negative $\delta^{18}O_{atm}$ and CH$_4$>600 ppb are not compatible with any other

414   age in the past 200 kyr other than the LIG at around 122 ka, and a short period in the Holocene at 7

415   ka. These datapoints are also incompatible with any mixtures of ice from other depths. Because the

416   data point at 615.3 m is compatible with a range of ages, we choose a conservative range of depths

417   from 617 m (just above the clear match at 618.3 m) to 628 m where we are very confident that we

418   have a sequence of ice from the last interglacial, covering the period 126 ka to 117 ka. Although it

419   lies within the uncertainty of the values at 627.3 m, the data point at 630.3 m (shown in red) is also

420   only consistent with the last interglacial, but does not show the expected increase in age with depth,

421   and could show a reversal in age. As this is already in the section that appears disturbed in methane

422   and $\delta^{18}O_{ice}$, we consider this data point and the ice around it as subject to disturbance.

423
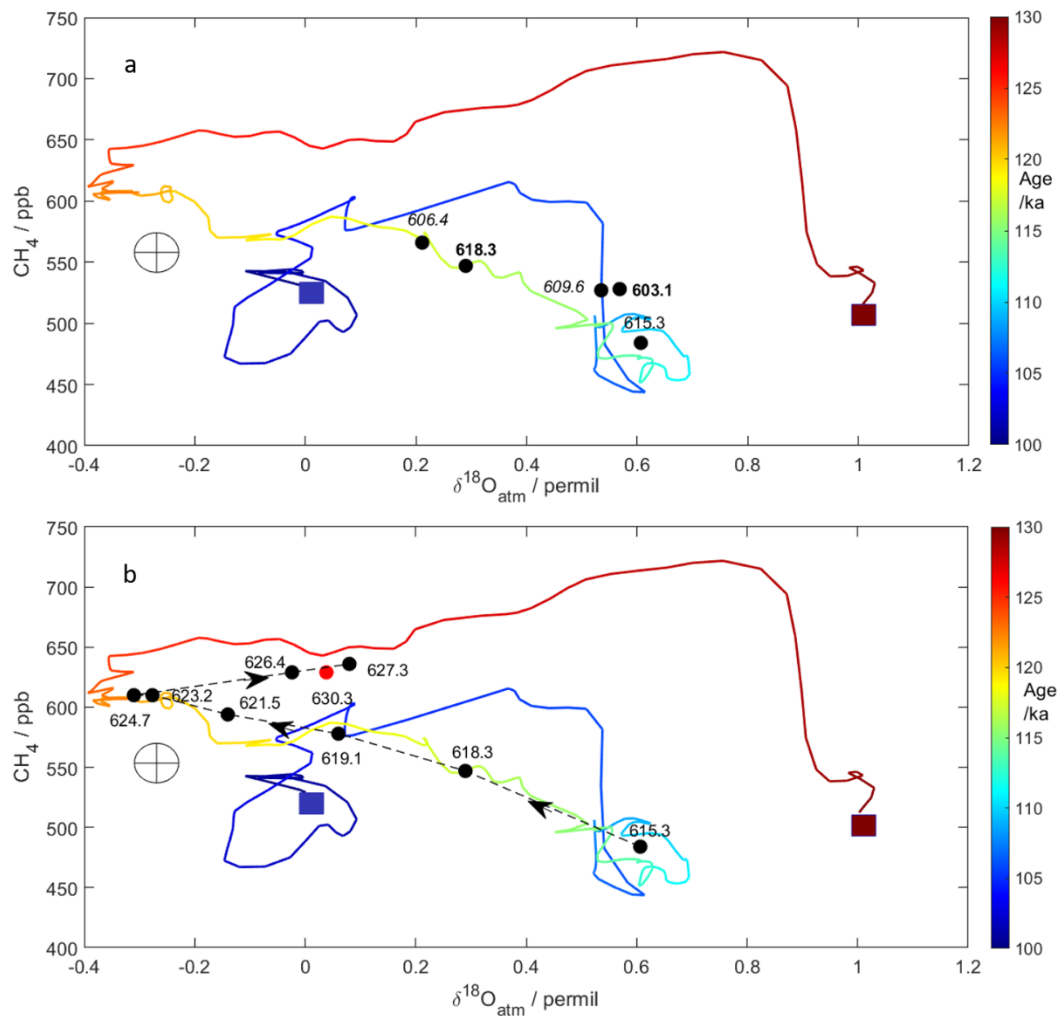
Figure 9. Cross plots of CH$_4$ (Köhler et al., 2017) and δ^{18}O$_{atm}$ (Extier et al., 2018) reference data for the period 100-130 ka, along with Skytrain Ice Rise data from (a) 603-618 m depth and (b) 615-628 m (black dots) and 630.3 m (red dot). The combined uncertainty (used to decide whether a match between the Skytrain and reference data is acceptable) is shown by the grey ellipse/cross. The start (130 ka) and end (100 ka) of the reference curve are marked by red and blue squares. Skytrain data points are marked with depths; in panel (a) the ones we later judge as being in disturbed ice are marked with italics, while the ones we consider well-dated are in bold. In panel b, the black dots are joined by dashed line with arrows pointing in order of increasing depth. An alternative visualisation of this figure is provided in Fig. S6.

Finally, we examine the data from 630 m to 635 m (Fig. 10). The point at 631.6, sitting close to clearly disturbed ice with rapidly changing values of CH$_4$ and δ^{18}O$_{ice}$, has values not seen in the reference data, and is probably a mixture of interglacial and glacial ice. The other data have values consistent with ages that would occur in the middle of MIS6 (140-180 ka), or alternatively could originate from ice that is much older (from an earlier glacial cycle). Because there are a number of

19

440   age solutions within the uncertainty of the measurements we do not attempt to assign ages to these

441   data points.

442
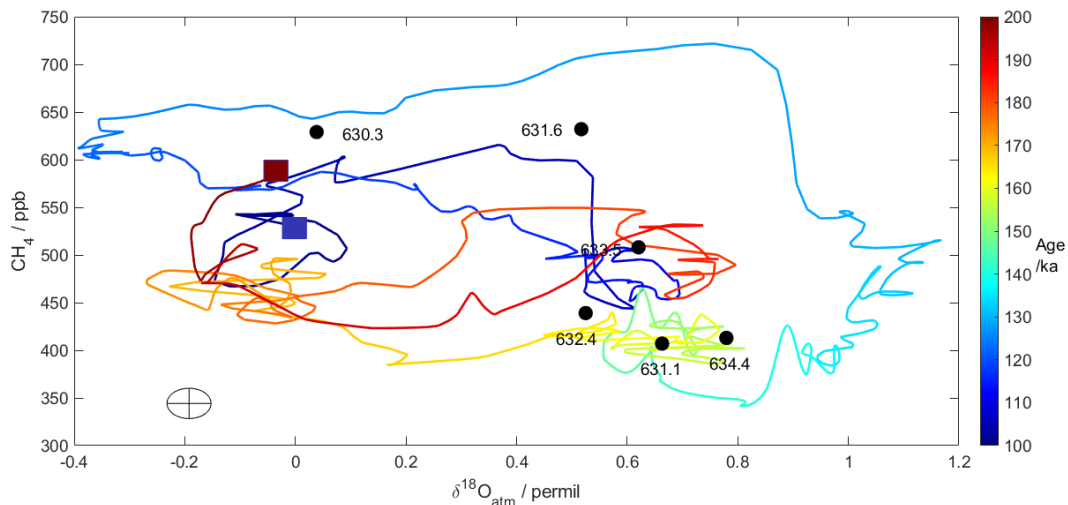
Figure 10. Cross plot of CH_4 (Köhler et al., 2017; Loulergue et al., 2008) and $\delta^{18}O_{atm}$ (Extier et al., 2018) reference data for the period 100-200 ka. The colourbar indicates the age of the sample. Also shown are the Skytrain data from 630 m downwards (black dots). The combined uncertainty (used to decide whether a match between the Skytrain and reference data is acceptable) is shown by the grey ellipse/cross. The start (200 ka) and end (100 ka) of the reference curve are marked by red and blue squares. An alternative visualisation of this figure is provided in Fig. S7.

449

450   6.2. Stratigraphy around the LIG

451   Combining the observation that no ice has methane values that fit in the age ranges 127-129 ka or

452   ~140 ka, and the positive identification of ice with unique combinations of CH_4 and $\delta^{18}O_{atm}$, we

453   conclude the following:

454   a) there is probably a flow disturbance at the top of the last interglacial section, with ice from ~106-

455   117 ka repeated;

456   b) despite this, there is a continuous section of ice from 617-628 m that represents the time period

457   from 117-126 ka in good order;

458   c) there is strongly disturbed ice at the base of the LIG section, with the ice below it most likely

459   representing much older ice from MIS6 or beyond.

460

461   7.   Application of Paleochrono

462   The Paleochrono model was run using the prior constraints discussed in section 2 and the tie points

463   described in section 5 (and shown in Table S3 and S4). For the section deeper than 600 m we have

464   assigned tie points based on CH$_4$ and δ^{18}O$_{atm}$ that anchor 603 m at 106 ka, and ties for each

465   CH$_4$/δ^{18}O$_{atm}$ pair between 617 and 627.3 m (117-126 ka). We then assigned a much older age to 632

466   m just to allow continuity of the age scale to the bed. No other tie points were applied below 628 m

467   (126 ka), and the ice ages below that were ignored. Between the tie points at 603 and 618 m,

468   Paleochrono assigns ages but because we know that there is disturbance and likely repeated ice, we

469   cannot trust all of them. As a compromise, in our age scale we report the ages as far as 605 m (108.7

470   ka) and from 617 m (~117 ka) but do not show any ages for 605-617 m. The age model is reported

471   with both ice age and gas age, along with uncertainties derived from the model. Fig. 11 shows the

472   depth-age relationship (continuous line) from the model. A depth-age lookup table is supplied in the

473   supplement. Methane and nssMg data are shown on the derived age model to 126 ka in Figs. 5 and

474   7. We have placed a grey bar on data in the disturbed section (605-617 m) where ages cannot be

475   considered reliable.
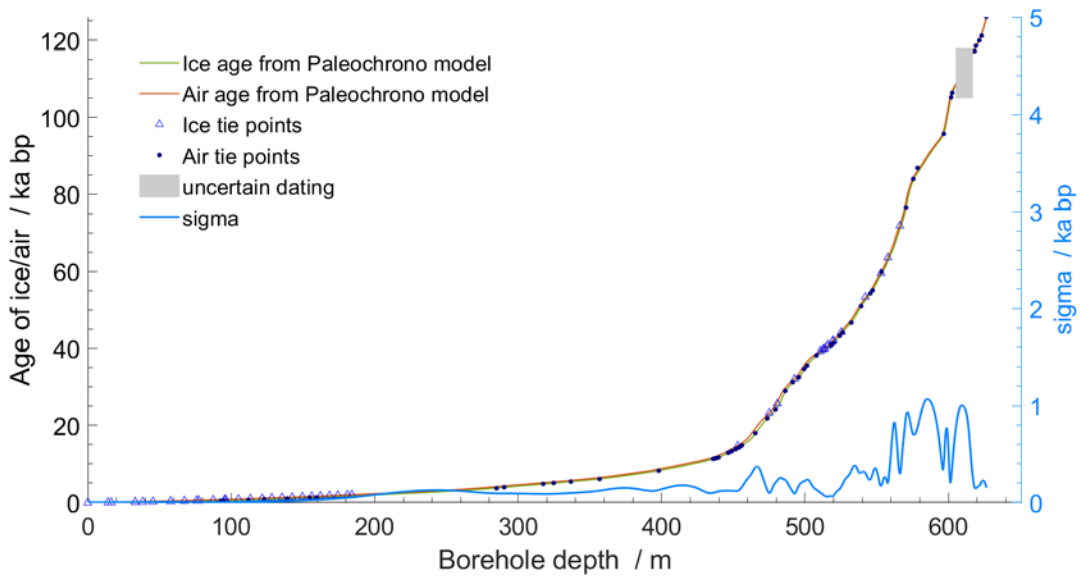
476

477   Figure 11. Age against depth for the Skytrain Ice Rise ice core. In the top panel, Ice and air age are

478   shown, along with the tie points we applied. The turquoise line shows the uncertainty on the ice age

479   derived from Paleochrono, using the right hand y-axis. The section with unreliable ages (605-617 m)

480   is greyed out, and the uncertainties around this section are probably underestimated.

481   In the supplement we present the deposition rate (Fig S2), thinning function (Fig. S3) and annual

482   layer thickness (Fig. S4) derived from the model. No dramatic deviations are seen, indicating that the

483   derived age model is physically reasonable. However given the flow disturbances beyond 605 m the

484   derived values may be unreliable from 605 m to the bed.

485   To further assess the age assignments around the LIG, in Fig. 12 we show the values of discrete

486   measurements of CH_4 and $\delta^{18}O_{atm}$ with the ages from Paleochrono for the sections of ice we

487   consider less disturbed. It can be seen that both the values and sequence for both parameters are

488   consistent, and generally match the reference data within uncertainty between 117 and 126 ka.

489   Although Palechrono separated them in order to maintain continuity, the data points (at 626.4 and

490   627.3 m), showing as slightly displaced from the reference curves at 125 and 127 ka in Fig. 12, were

491   originally both assigned tie point ages of ~126 ka, which would also place them on the reference

492   curves.
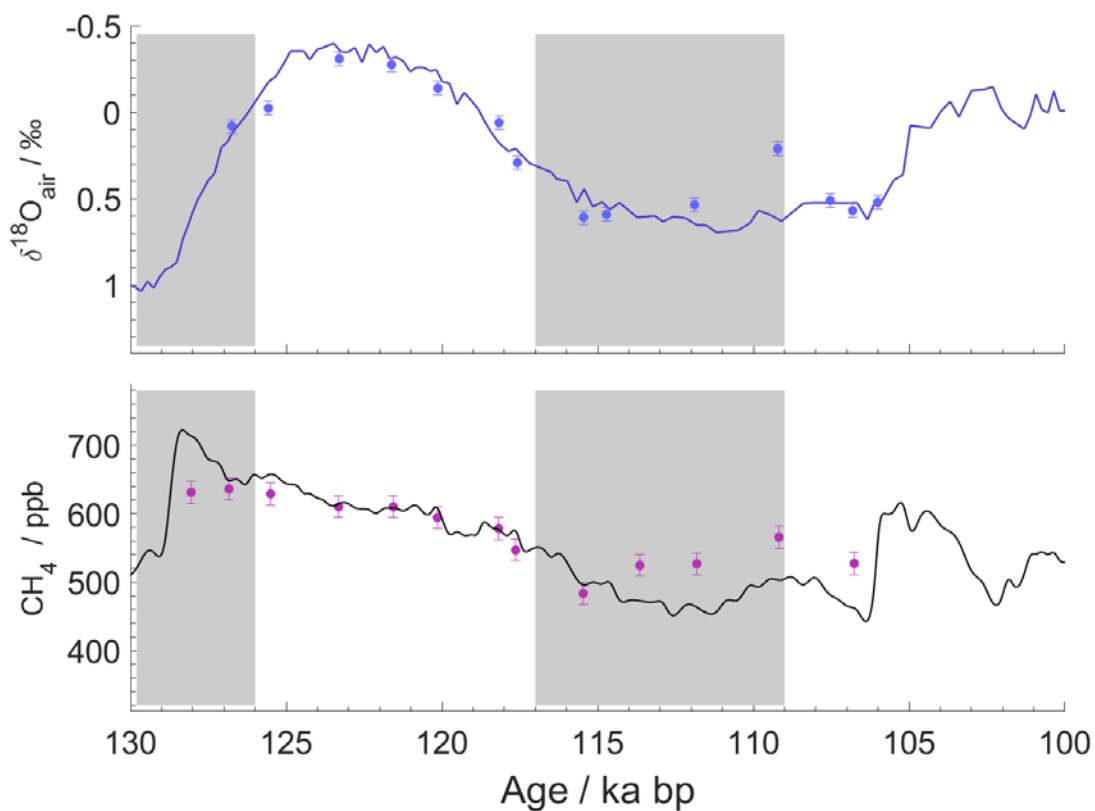
493

494   Figure 12: Reference data for CH_4 and $\delta^{18}O_{atm}$ between 100 and 130 ka (as in Fig. 8a), along with

495   discrete measurements (symbols) for the Skytrain Ice Rise ice core. Sections with unreliable ages

496   (605-617 m and >627 m) are greyed out. The error bars are the combined uncertainty (at 1 sigma) of

497   the Skytrain and reference data.

498   8.   Disturbed ice around the LIG

499   It is evident that there is ice disturbance both at the top, and particularly at the base, of the LIG.

500   Such disturbances have been observed in previous LIG ice, though until now only documented in

22

501 Greenland ice (Grootes et al., 1993; NEEM Community Members, 2013). Such discontinuities have

502 been hypothesised to result from the contrast between ice layers with very different rheological

503 properties, due to changes in impurity content and grain size (LIG versus Penultimate Glacial

504 Maximum (PGM) and LIG versus late MIS 5) (NEEM Community Members, 2013). We expect smaller

505 contrasts in properties in Antarctica compared to Greenland.

506 We do not have enough evidence to conclude whether the disturbance we see is indeed due to

507 rheoogical contrasts or is just a consequence of investigating ice that is close to the bed. A tendency

508 to become disturbed and folded might be exacerbated at Skytrain Ice Rise by the existence of a

509 rather large Raymond arch (Mulvaney et al., 2021), a dynamic feature seen in the radar profiles,

510 extending right to the bed (the internal layering (Mulvaney et al., 2021) shows upwarping of order

511 50 m within around 1 km horizontal distance only 100 m above the bed). Although we expect

512 Skytrain Ice rise to have remained a separate flow centre, it is likely that the position of the dome

513 was different during the LGM when the Ronne Ice Shelf would have been grounded and provided

514 greater restraint to the north and east; this could also have led to disturbance around the LIG ice

515 which would already have been deep in the ice column at that time.

516 We consider here possible alternative causes for the hiatus, with ice from 127-129 ka missing from

517 our sequence, and probably ice from 129 to at least 140 ka also unrepresented.

518 a) The first possibility is that there was no snow accumulation during this period. This is

519 considered extremely unlikely. The section from 127-129 ka at other Antarctic sites shows

520 high temperatures and inferred high accumulation rates.

521 b) A second possibility is that the ice from inland overrode Skytrain Ice rise causing some layers

522 to be removed completely. However, the Ellsworth Mountains provide a high and rather

523 solid barrier against such flow. There is also no sign of ice anywhere in the core with the

524 much more negative water isotopic contents one would expect from ice originating at much

525 higher altitude inland.

526 c) Some ice sheet models have inferred a possible loss of ice from parts of WAIS during the LIG

527 (DeConto and Pollard, 2016). This hypothesis raises the possibility that ice was completely

528 lost from Skytrain Ice Rise in the warmest part of the LIG. However, the existence of more

529 than 20 m of ice that appears to derive from MIS6 or older suggests that ice was not

530 completely removed from Skytrain Ice rise. In addition if some ice was lost by melting, while

531 older ice was retained, we would expect to see bubble-free ice (caused by refreezing after

532 melting). This is not observed anywhere in the core: normal values of total air content and

533 methane concentrations are seen at all depths.

534   We therefore conclude that the most plausible explanation for our observations is flow

535   disturbance due to contrasting rheology. However, detailed ice sheet modelling, as well as

536   rheological studies on the Skytrain ice core, are required to firmly rule out other causes.

537

538 9. Conclusion

539 We have constructed an age model, which we call ST22, for the Skytrain Ice Rise ice core. This age

540 model is based mainly on tie points to previous Antarctic ice cores, using a range of analyses. The

541 age-depth relationship is well-behaved until at least 100 ka. There appears to be flow disturbance at

542 the top of the LIG section, but the core contains ice from the last interglacial (117 to 126 ka) in good

543 stratigraphic order. It is however missing the earliest part of the LIG, and the coldest part of the

544 PGM, apparently also due to flow disturbance affecting ice layers with contrasting rheologies.

545 Because the missing ice appears to have been affected by flow disturbances, we surmise that

546 another core at a suitably chosen location on Skytrain Ice rise might be capable of retrieving ice from

547 the missing sections. This is the first time that flow disturbances around the LIG have been clearly

548 documented for Antarctica, as they have been several times for Greenland. These disturbances raise

549 the possibility that such disturbances might also have affected other records of the LIG (Korotkikh et

550 al., 2011). One obvious conclusion from our data is that the ice sheet was certainly present at

551 Skytrain Ice Rise during the LIG.

552 **Data availability**

553 The continuous methane and nssMg used in this paper (and shown in Figs 5 and 7) are available at

554 Pangaea (https://doi.pangaea.de/10.1594/PANGAEA.956062). The discrete CH_4, $\delta^{18}O_{atm}$ and ^{10}Be

555 data used in this paper are attached as supplementary data (Tables S1 and S2). The air and ice tie

556 points used in Paleochrono are attached as supplementary data (Tables S3 and S4). All reference

557 data used in this paper are already published and available online. The final derived age model ST22

558 is attached as supplementary table S5, and is available at Pangaea

559 (https://doi.pangaea.de/10.1594/PANGAEA.956061).

560 **Author contributions**

561 The first two authors contributed equally to this paper. The paper was written by RMul and EW with

562 contributions mainly from HH, MG and RR. The ice core was drilled and sectioned by EW, RMul, CN-

563 A, MG, IR. The CFA analysis was performed by HH, MG, JH, RMul, RR and IR. Discrete methane

564 analyses were provided by LS, HF and TS; $\delta^{18}O_{atm}$ data were provided by FP and AL; ^{10}Be data were

565 provided by MC and RMus. RMul ran Paleochrono with advice from FP. All authors contributed to
566 improving the final paper.

Competing interests

Acknowledgments

References

583 Adolphi, F., Bronk Ramsey, C., Erhardt, T., Edwards, R. L., Cheng, H., Turney, C. S. M., Cooper, A.,
584 Svensson, A., Rasmussen, S. O., Fischer, H., and Muscheler, R.: Connecting the Greenland ice-core
585 and U∕Th timescales via cosmogenic radionuclides: testing the synchroneity of Dansgaard–Oeschger
586 events, Clim. Past, 14, 1755-1781, doi: 10.5194/cp-14-1755-2018, 2018.

588 Adolphi, F. and Muscheler, R.: Synchronizing the Greenland ice core and radiocarbon timescales over
589 the Holocene – Bayesian wiggle-matching of cosmogenic radionuclide records, Clim. Past, 12, 15-30,
590 doi: 10.5194/cp-12-15-2016, 2016.

592 Ahn, J. and Brook, E. J.: Atmospheric CO_2 and climate on millennial time scales during the last glacial
593 period, Science, 322, 83-85, doi: 10.1126/science.1160832, 2008.

595 Baggenstos, D., Severinghaus, J. P., Mulvaney, R., McConnell, J. R., Sigl, M., Maselli, O., Petit, J. R.,
596 Grente, B., and Steig, E. J.: A Horizontal Ice Core From Taylor Glacier, Its Implications for Antarctic
597 Climate History, and an Improved Taylor Dome Ice Core Time Scale, Paleoceanography and
598 Paleoclimatology, 33, 778-794, doi: 10.1029/2017pa003297, 2018.

600 Baumgartner, M., Kindler, P., Eicher, O., Floch, G., Schilt, A., Schwander, J., Spahni, R., Capron, E.,
601 Chappellaz, J., Leuenberger, M., Fischer, H., and Stocker, T. F.: NGRIP CH_4 concentration from 120 to

602 10 kyr before present and its relation to a delta N-15 temperature reconstruction from the same ice
603 core, Climate of the Past, 10, 903-920, doi: 10.5194/cp-10-903-2014, 2014.

604

605 Bazin, L., Landais, A., Lemieux-Dudon, B., Kele, H. T. M., Veres, D., Parrenin, F., Martinerie, P., Ritz, C.,
606 Capron, E., Lipenkov, V., Loutre, M. F., Raynaud, D., Vinther, B., Svensson, A., Rasmussen, S. O.,
607 Severi, M., Blunier, T., Leuenberger, M., Fischer, H., Masson-Delmotte, V., Chappellaz, J., and Wolff,
608 E. W.: An optimised multi-proxy, multi-site Antarctic ice and gas orbital chronology (AICC2012): 120-
609 800 ka, Climate of the Past 9, 1715-1731, 2013.

610

611 Brook, E. J., White, J. W. C., Schilla, A. S. M., Bender, M. L., Barnett, B., Severinghaus, J. P., Taylor, K.
612 C., Alley, R. B., and Steig, E. J.: Timing of millennial-scale climate change at Siple Dome, West
613 Antarctica, during the last glacial period, Quat. Sci. Rev., 24, 1333-1343, 2005.

614

615 Buizert, C., Cuffey, K. M., Severinghaus, J. P., Baggenstos, D., Fudge, T. J., Steig, E. J., Markle, B. R.,
616 Winstrup, M., Rhodes, R. H., Brook, E. J., Sowers, T. A., Clow, G. D., Cheng, H., Edwards, R. L., Sigl, M.,
617 McConnell, J. R., and Taylor, K. C.: The WAIS Divide deep ice core WD2014 chronology - Part 1:
618 Methane synchronization (68-31 kaBP) and the gas age-ice age difference, Climate of the Past, 11,
619 153-173, doi: 10.5194/cp-11-153-2015, 2015.

620

621 Buizert, C., Sigl, M., Severi, M., Markle, B. R., Wettstein, J. J., McConnell, J. R., Pedro, J. B.,
622 Sodemann, H., Goto-Azuma, K., Kawamura, K., Fujita, S., Motoyama, H., Hirabayashi, M., Uemura, R.,
623 Stenni, B., Parrenin, F., He, F., Fudge, T. J., and Steig, E. J.: Abrupt ice-age shifts in southern westerly
624 winds and Antarctic climate forced from the north, Nature, 563, 681-685, doi: 10.1038/s41586-018-
625 0727-5, 2018.

626

627 Capron, E., Landais, A., Lemieux-Dudon, B., Schilt, A., Masson-Delmotte, V., Buiron, D., Chappellaz, J.,
628 Dahl-Jensen, D., Johnsen, S., Leuenberger, M., Loulergue, L., and Oerter, H.: Synchronising EDML and
629 NorthGRIP ice cores using $\delta^{18}O$ of atmospheric oxygen ($\delta^{18}O_{atm}$) and CH_4 measurements over MIS 5
630 (80-123 ka), Quat. Sci. Rev., 29, 222-234, 2010.

631

632 Chappellaz, J., Brook, E., Blunier, T., and Malaizé, B.: CH4 and delta O-18 of O-2 records from
633 Antarctic and Greenland ice: A clue for stratigraphic disturbance in the bottom part of the Greenland
634 Ice Core Project and the Greenland Ice Sheet Project 2 ice cores, J. Geophys. Res., 102, 26547-26557,
635 1997.

636

637 Christl, M., Vockenhuber, C., Kubik, P. W., Wacker, L., Lachner, J., Alfimov, V., and Synal, H. A.: The
638 ETH Zurich AMS facilities: Performance parameters and reference materials, Nuclear Instruments
639 and Methods in Physics Research Section B: Beam Interactions with Materials and Atoms, 294, 29-
640 38, doi: https://doi.org/10.1016/j.nimb.2012.03.004, 2013.

641

642 Crotti, I., Landais, A., Stenni, B., Bazin, L., Parrenin, F., Frezzotti, M., Ritterbusch, F., Lu, Z.-T., Jiang,
643 W., Yang, G.-M., Fourré, E., Orsi, A., Jacob, R., Minster, B., Prié, F., Dreossi, G., and Barbante, C.: An
644 extension of the TALDICE ice core age scale reaching back to MIS 10.1, Quat. Sci. Rev., 266, 107078,
645 doi: https://doi.org/10.1016/j.quascirev.2021.107078, 2021.

646

647 DeConto, R. M. and Pollard, D.: Contribution of Antarctica to past and future sea-level rise, Nature,
648 531, 591-597, doi: 10.1038/nature17145, 2016.

649

650 DeConto, R. M., Pollard, D., Alley, R. B., Velicogna, I., Gasson, E., Gomez, N., Sadai, S., Condron, A.,
651 Gilford, D. M., Ashe, E. L., Kopp, R. E., Li, D., and Dutton, A.: The Paris Climate Agreement and future
652 sea-level rise from Antarctica, Nature, 593, 83-89, doi: 10.1038/s41586-021-03427-0, 2021.

653

654 Dutton, A., Carlson, A. E., Long, A. J., Milne, G. A., Clark, P. U., DeConto, R., Horton, B. P., Rahmstorf,
655 S., and Raymo, M. E.: Sea-level rise due to polar ice-sheet mass loss during past warm periods,
656 Science, 349, 153-+, doi: 10.1126/science.aaa4019, 2015.

657

658 Dyer, B., Austermann, J., D'Andrea, W. J., Creel, R. C., Sandstrom, M. R., Cashman, M., Rovere, A.,
659 and Raymo, M. E.: Sea-level trends across The Bahamas constrain peak last interglacial ice melt,
660 Proceedings of the National Academy of Sciences, 118, e2026839118, doi:
661 10.1073/pnas.2026839118, 2021.

662

663 EPICA Community Members: Eight glacial cycles from an Antarctic ice core, Nature, 429, 623-628,
664 doi: 10.1038/nature02599, 2004.

665

666 Epifanio, J. A., Brook, E. J., Buizert, C., Edwards, J. S., Sowers, T. A., Kahle, E. C., Severinghaus, J. P.,
667 Steig, E. J., Winski, D. A., Osterberg, E. C., Fudge, T. J., Aydin, M., Hood, E., Kalk, M., Kreutz, K. J.,
668 Ferris, D. G., and Kennedy, J. A.: The SP19 chronology for the South Pole Ice Core – Part 2: gas
669 chronology, Δage, and smoothing of atmospheric records, Clim. Past, 16, 2431-2444, doi:
670 10.5194/cp-16-2431-2020, 2020.

671

672 Extier, T., Landais, A., Bréant, C., Prié, F., Bazin, L., Dreyfus, G., Roche, D. M., and Leuenberger, M.:
673 On the use of δ18Oatm for ice core dating, Quat. Sci. Rev., 185, 244-257, doi:
674 https://doi.org/10.1016/j.quascirev.2018.02.008, 2018.

675

676 Fischer, H., Fundel, F., Ruth, U., Twarloh, B., Wegner, A., Udisti, R., Becagli, S., Castellano, E.,
677 Morganti, A., Severi, M., Wolff, E. W., Littot, G. C., Rothlisberger, R., Mulvaney, R., Hutterli, M. A.,
678 Kaufmann, P., Federer, U., Lambert, F., Bigler, M., Hansson, M., Jonsell, U., de Angelis, M., Gabrielli,
679 P., Boutron, C., Siggaard-Andersen, M. L., Steffensen, J. P., Barbante, C., Gaspari, V., and Wagenbach,
680 D.: Reconstruction of millennial changes in transport, dust emission and regional differences in sea
681 ice coverage using the deep EPICA ice cores from the Atlantic and Indian Ocean sector of Antarctica.,
682 Earth planet. Sci. Lett., 260, 340-354, 2007.

683

684 Fox-Kemper, B., Hewitt, H., Xiao, C., Aðalgeirsdóttir, G., Drijfhout, S. S., Edwards, T. L., Golledge, N.
685 R., Hemer, M., Kopp, R. E., Krinner, G., Mix, A., Notz, D., Nowicki, S., Nurhati, I. S., Ruiz, L., Sallée, J.-
686 B., Slangen, A. B. A., and Yu, Y.: Chapter 9: Ocean, Cryosphere and Sea Level Change. In: Climate
687 Change 2021: The Physical Science Basis. Contribution of Working Group I to the Sixth Assessment
688 Report of the Intergovernmental Panel on Climate Change, Masson-Delmotte, V., Zhai, P., Pirani, A.,
689 Connors, S. L., Péan, C., Berger, S., Caud, N., Chen, Y., Goldfarb, L., Gomis, M. I., Huang, M., Leitzell,
690 K., Lonnoy, E., Matthews, J. B. R., Maycock, T. K., Waterfield, T., Yelekçi, O., Yu, R., and Zhou, B.
691 (Eds.), Cambridge University Press, 2021.

692

693 Gilford, D. M., Ashe, E. L., DeConto, R. M., Kopp, R. E., Pollard, D., and Rovere, A.: Could the Last
694 Interglacial Constrain Projections of Future Antarctic Ice Mass Loss and Sea-Level Rise?, Journal of
695 Geophysical Research: Earth Surface, 125, e2019JF005418, doi:
696 https://doi.org/10.1029/2019JF005418, 2020.

697

698 Grieman, M. M., Hoffmann, H. M., Humby, J. D., Mulvaney, R., Nehrbass-Ahles, C., Rix, J., Thomas, E.
699 R., Tuckwell, R., and Wolff, E. W.: Continuous flow analysis methods for sodium, magnesium and
700 calcium detection in the Skytrain ice core, J. Glaciol., 68, 90-100, doi: 10.1017/jog.2021.75, 2021.

701

702 Grootes, P. M., Steig, E. J., Stuiver, M., Waddington, E. D., and Morse, D. L.: The Taylor dome
703 antarctic O-18 record and globally synchronous changes in climate, Quaternary Res., 56, 289-298,
704 2001.

705

706 Grootes, P. M., Stuiver, M., White, J. W. C., Johnsen, S., and Jouzel, J.: Comparison of oxygen isotope
707 records from the GISP2 and GRIP Greenland ice cores, Nature, 366, 552-554, 1993.

708

709 Hoffmann, H. M., Grieman, M. M., King, A. C. F., Epifanio, J. A., Martin, K., Vladimirova, D., Pryer, H.
710 V., Doyle, E., Schmidt, A., Humby, J. D., Rowell, I. F., Nehrbass-Ahles, C., Thomas, E. R., Mulvaney, R.,
711 and Wolff, E. W.: The ST22 chronology for the Skytrain Ice Rise ice core – Part 1: A stratigraphic
712 chronology of the last 2000 years, Clim. Past, 18, 1831-1847, doi: 10.5194/cp-18-1831-2022, 2022.

713

714 Jacobel, R. W., Welch, B. C., Steig, E. J., and Schneider, D. P.: Glaciological and climatic significance of
715 Hercules Dome, Antarctica: An optimal site for deep ice core drilling, J. Geophys. Res.-Earth Surf.,
716 110, doi: 10.1029/2004jf000188, 2005.

717

718 Kawamura, K., Parrenin, F., Lisiecki, L., Uemura, R., Vimeux, F., Severinghaus, J. P., Hutterli, M. A.,
719 Nakazawa, T., Aoki, S., Jouzel, J., Raymo, M. E., Matsumoto, K., Nakata, H., Motoyama, H., Fujita, S.,
720 Azuma, K., Fujii, Y., and Watanabe, O.: Northern Hemisphere forcing of climatic cycles over the past
721 360,000 years implied by accurately dated Antarctic ice cores, Nature, 448, 912-916, 2007.

722

723 Köhler, P., Nehrbass-Ahles, C., Schmitt, J., Stocker, T. F., and Fischer, H.: A 156 kyr smoothed history
724 of the atmospheric greenhouse gases CO_2, CH_4, and N_2O and their radiative forcing, Earth Syst. Sci.
725 Data, 9, 363-387, doi: 10.5194/essd-9-363-2017, 2017.

726

727 Korotkikh, E. V., Mayewski, P. A., Handley, M. J., Sneed, S. B., Introne, D. S., Kurbatov, A. V., Dunbar,
728 N. W., and McIntosh, W. C.: The last interglacial as represented in the glaciochemical record from
729 Mount Moulton Blue Ice Area, West Antarctica, Quat. Sci. Rev., 30, 1940-1947, 2011.

730

731 Lee, J. E., Brook, E. J., Bertler, N. A. N., Buizert, C., Baisden, T., Blunier, T., Ciobanu, V. G., Conway, H.,
732 Dahl-Jensen, D., Fudge, T. J., Hindmarsh, R., Keller, E. D., Parrenin, F., Severinghaus, J. P., Vallelonga,
733 P., Waddington, E. D., and Winstrup, M.: An 83000-year-old ice core from Roosevelt Island, Ross Sea,
734 Antarctica, Clim. Past, 16, 1691-1713, doi: 10.5194/cp-16-1691-2020, 2020.

735

736 Loulergue, L., Schilt, A., Spahni, R., Masson-Delmotte, V., Blunier, T., Lemieux, B., Barnola, J. M.,
737 Raynaud, D., Stocker, T. F., and Chappellaz, J.: Orbital and millennial-scale features of atmospheric
738 CH_4 over the last 800,000 years, Nature, 453, 383-386, 2008.

739

740 Matsuoka, K., Skoglund, A., Roth, G., de Pomereu, J., Griffiths, H., Headland, R., Herried, B.,
741 Katsumata, K., Le Brocq, A., Licht, K., Morgan, F., Neff, P. D., Ritz, C., Scheinert, M., Tamura, T., Van
742 de Putte, A., van den Broeke, M., von Deschwanden, A., Deschamps-Berger, C., Van Liefferinge, B.,
743 Tronstad, S., and Melvær, Y.: Quantarctica, an integrated mapping environment for Antarctica, the
744 Southern Ocean, and sub-Antarctic islands, Environmental Modelling & Software, 140, 105015, doi:
745 https://doi.org/10.1016/j.envsoft.2021.105015, 2021.

746

747 Mitchell, L., Brook, E., Lee, J. E., Buizert, C., and Sowers, T.: Constraints on the Late Holocene
748 Anthropogenic Contribution to the Atmospheric Methane Budget, Science, 342, 964-966, doi:
749 10.1126/science.1238920, 2013.

750

751 Mulvaney, R., Alemany, O., and Possenti, P.: The Berkner Island ice core drilling project, Ann.
752 Glaciol., 47, 115-124, 2007.

753

754 Mulvaney, R., Rix, J., Polfrey, S., Grieman, M., Martìn, C., Nehrbass-Ahles, C., Rowell, I., Tuckwell, R.,
755 and Wolff, E.: Ice drilling on Skytrain Ice Rise and Sherman Island, Antarctica, Ann. Glaciol., 62, 311-
756 323, doi: 10.1017/aog.2021.7, 2021.

757

758 Mulvaney, R., Röthlisberger, R., Wolff, E. W., Sommer, S., Schwander, J., Hutterli, M. A., and Jouzel,
759 J.: The transition from the last glacial period in inland and near-coastal Antarctica, Geophys. Res.
760 Lett., 27, 2673-2676, 2000.

761

762 Mulvaney, R., Triest, J., and Alemany, O.: The James Ross Island and the Fletcher Promontory ice-
763 core drilling projects, Ann. Glaciol., 55, 179-188, doi: 10.3189/2014AoG68A044, 2014.

764

765 NEEM Community Members: Eemian interglacial reconstructed from a Greenland folded ice core
766 Nature, 493, 489-494, doi: 10.1038/nature11789, 2013.

767

768 Parrenin, F., Bazin, L., Capron, E., Landais, A., Lemieux-Dudon, B., and Masson-Delmotte, V.:
769 IceChrono1: a probabilistic model to compute a common and optimal chronology for several ice
770 cores, Geosci. Model Dev., 8, 1473-1492, doi: 10.5194/gmd-8-1473-2015, 2015.

771

772 Raisbeck, G. M., Cauquoin, A., Jouzel, J., Landais, A., Petit, J. R., Lipenkov, V. Y., Beer, J., Synal, H. A.,
773 Oerter, H., Johnsen, S. J., Steffensen, J. P., Svensson, A., and Yiou, F.: An improved north–south
774 synchronization of ice core records around the 41 kyr 10Be peak, Clim. Past, 13, 217-229, doi:
775 10.5194/cp-13-217-2017, 2017.

776

777 Rhodes, R. H., Brook, E. J., Chiang, J. C. H., Blunier, T., Maselli, O. J., McConnell, J. R., Romanini, D.,
778 and Severinghaus, J. P.: Enhanced tropical methane production in response to iceberg discharge in
779 the North Atlantic, Science, 348, 1016-1019, doi: 10.1126/science.1262005, 2015.

780

781 Rhodes, R. H., Brook, E. J., McConnell, J. R., Blunier, T., Sime, L. C., Faïn, X., and Mulvaney, R.:
782 Atmospheric methane variability: Centennial-scale signals in the Last Glacial Period, Global
783 Biogeochemical Cycles, 31, 575-590, doi: 10.1002/2016GB005570, 2017.

784

785 Röthlisberger, R., Mulvaney, R., Wolff, E. W., Hutterli, M., Bigler, M., Sommer, S., and Jouzel, J.: Dust
786 and sea salt variability in central East Antarctica (Dome C) over the last 45 kyrs and its implications
787 for southern high-latitude climate, Geophys. Res. Lett., 29, 1963, doi: doi:10.1029/2002GL015186,
788 2002.

789

790 Saltzman, E. S., Dioumaeva, I., and Finley, B. D.: Glacial/interglacial variations in methanesulfonate
791 (MSA) in the Siple Dome ice core, West Antarctica, Geophys. Res. Lett., 33, 2006.

792

793 Schmidely, L., Nehrbass-Ahles, C., Schmitt, J., Han, J., Silva, L., Shin, J., Joos, F., Chappellaz, J., Fischer,
794 H., and Stocker, T. F.: CH4 and N2O fluctuations during the penultimate deglaciation, Clim. Past, 17,
795 1627-1643, doi: 10.5194/cp-17-1627-2021, 2021.

796

797 Severinghaus, J. P., Beaudette, R., Headly, M. A., Taylor, K., and Brook, E. J.: Oxygen-18 of O_2 Records
798 the Impact of Abrupt Climate Change on the Terrestrial Biosphere, Science, 324, 1431-1434, doi:
799 10.1126/science.1169473, 2009.

800

801 Sigl, M., Fudge, T. J., Winstrup, M., Cole-Dai, J., Ferris, D., McConnell, J. R., Taylor, K. C., Welten, K. C.,
802 Woodruff, T. E., Adolphi, F., Bisiaux, M., Brook, E. J., Buizert, C., Caffee, M. W., Dunbar, N. W.,
803 Edwards, R., Geng, L., Iverson, N., Koffman, B., Layman, L., Maselli, O. J., McGwire, K., Muscheler, R.,
804 Nishiizumi, K., Pasteris, D. R., Rhodes, R. H., and Sowers, T. A.: The WAIS Divide deep ice core
805 WD2014 chronology – Part 2: Annual-layer counting (0–31 ka BP), Clim. Past, 12, 769-786, doi:
806 10.5194/cp-12-769-2016, 2016.

807

808 Sigl, M., Toohey, M., McConnell, J. R., Cole-Dai, J., and Severi, M.: Volcanic stratospheric sulfur
809 injections and aerosol optical depth during the Holocene (past 11,500 years) from a bipolar ice core
810 array, Earth Syst. Sci. Data Discuss., 2022, 1-45, doi: 10.5194/essd-2021-422, 2022.

811

812 Veres, D., Bazin, L., Landais, A., Kele, H. T. M., Lemieux-Dudon, B., Parrenin, F., Martinerie, P., Blayo,
813 E., Blunier, T., Capron, E., Chappellaz, J., Rasmussen, S. O., Severi, M., Svensson, A., Vinther, B., and
814 Wolff, E. W.: The Antarctic ice core chronology (AICC2012): an optimised multi-parameter and multi-
815 site dating approach for the last 120 thousand years, Climate of the Past, 9, 1733-1748, 2013.

816

817 Wolff, E. W., Barbante, C., Becagli, S., Bigler, M., Boutron, C. F., Castellano, E., De Angelis, M.,
818 Federer, U., Fischer, H., Fundel, F., Hansson, M., Hutterli, M., Jonsell, U., Karlin, T., Kaufmann, P.,
819 Lambert, F., Littot, G. C., Mulvaney, R., Rothlisberger, R., Ruth, U., Severi, M., Siggaard-Andersen, M.
820 L., Sime, L. C., Steffensen, J. P., Stocker, T. F., Traversi, R., Twarloh, B., Udisti, R., Wagenbach, D., and
821 Wegner, A.: Changes in environment over the last 800,000 years from chemical analysis of the EPICA
822 Dome C ice core, Quat. Sci. Rev., 29, 285-295, doi: 10.1016/j.quascirev.2009.06.013, 2010.

823

824 Yau, A. M., Bender, M. L., Robinson, A., and Brook, E. J.: Reconstructing the last interglacial at
825 Summit, Greenland: Insights from GISP2, Proc. Natl. Acad. Sci. U. S. A., 113, 9710-9715, doi:
826 10.1073/pnas.1524766113, 2016.

827

828